STScI | SPACE TELESCOPE SCIENCE INSTITUTE

Instrument Science Report STIS 2017-01(v1)

Status of the STIS Instrument Focus

Charles R. Proffitt, TalaWanda Monroe, and Linda Dressel

Space Telescope Science Institute, Baltimore, MD

12 January 2017

ABSTRACT

The Space Telescope Imaging Spectrograph needs to bring images to a good focus at its aperture plane and three detectors, for each of several optical paths. We discuss various ways of measuring the evolution of the focus over time for both the aperture plane and for a variety of imaging and spectroscopic modes. Evidence suggests that between 2013 and 2015 the best focus of STIS relative to the HST best focus, based on WFC3/UVIS and ACS/WFC monitoring, shifted by the equivalent of 3 microns of HST secondary motion, resulting in a decrease in the average small aperture throughput. We discuss the implications of this change for STIS observations.

Contents

1. Introduction

In the STIS instrument (Woodgate et al. 1998), the incoming beam needs to first be brought into focus at the aperture plane, and then again at the detector in use. Each of the three STIS detectors, CCD, FUV-MAMA, and NUV-MAMA is used with a number of optical elements, (mirrors or gratings), located in the Mode Select Mechanism (MSM). All modes share the same light path through the corrector mechanism and aperture plane up to the MSM, but after this the light path can differ significantly even for the various modes of the same detector. In principle all modes were adjusted to confocal with the aperture plane prior to launch, but this is not easy to verify in practice.

There are a few additional details that are useful to review before proceeding with a broader discussion of the history and current status of the STIS instrument focus. The STIS corrector mechanism provides the only way to tune the internal focus of any of the STIS optical paths and so we will first discuss its capabilities and prior use. The focus of *HST* itself changes over time and these variations and their uncertainties need to be taken into account before attempting to isolate any focus changes that may be unique to STIS. In addition, many STIS modes, including some of the ones most important for focus measurements, can be used with either clear or filtered apertures, and it is important to quantify the effect this has on focus measurements.

We will then discuss a variety of different measurements relevant to estimating the STIS focus qualilty. These include recent measurements of the throughputs of small apertures where recent measurements appear to show lower than expected throughput (§2), analysis of narrow-band OII images that are sensitive to focus offsets (§3), and autocorrelation techniques which can be used to directly measure changes in spectral resolution for both sharp-lined external targets as well as internal calibration line-lamp spectra (§4).

In §5 we will then discuss the impact of focus offsets on STIS data quality and science capablities, before summarizing in §6 our conclusions about the magnitude and causes of changes in the STIS focus over time.

1.1 The STIS Corrector Mechanism

The STIS corrector mechanism is based on the COSTAR mechanism (Kimble et al. 1998) and allows for +/- 5 mm adjustment in the focus direction as well as tip-tilt adjustment of +/- 32'. At the STIS aperture plane, 1 mm of corrector focus motion is equivalent to 915 motor steps (SER-STIS-MECH-126) and compensates for an *HST* secondary mirror motion of 9.1 μm, (Di Nino et al. 2003). During the 1997 Servicing Mission Observatory Verification (SMOV) period following STIS's installation during the 2nd *HST* servicing mission (SM2), the STIS corrector was adjusted by -796 motor steps (about 0.85 mm), from its initial launch position, while the X- and Y-tilt axis mechanisms were adjusted by +6 (~55.3") and -5 motor steps (~ 47.4"), respectively.

1.2 Observatory focus monitoring

The focus of *HST* changes over time, both due to a slow long-term shrinkage of the telescope truss and thermal "breathing" that changes the focus over orbital time scales. Phase retrieval techniques can be used to monitor the *HST* instrument focus (Krist & Burrows 1997). Since SM4, the overall *HST* observatory monitoring has primarily relied on images taken using the ACS WFC and the WFC3 UVIS. The long-term shrinkage is compensated for by occasional moves of the *HST* secondary mirror. STScI observatory support supplies a model of the focus, which includes both a long-term secular trend (Niemi et al 2010) and a short time-scale temperature based breathing model (Di Nino et al 2008), and also takes into account the history of secondary mirror moves. Results for this combined model of the focus have been tabulated at five-minute intervals, and are available back to March 9, 2003. Using focus monitoring data collected between March 2003 and January 2007, Cox & Niemi (2011) estimated that about 80% of the time this model produces results within 2 μm of the actual values, although offsets can occasionally be as large as 4 μm. However, some caution may be warranted in applying these results to current data, as the thermal environment of the telescope changed significantly after Servicing Mission 4 (SM4) and a detailed re-evaluation of the post-SM4 breathing model has yet to be published.

The shrinkage of the HST Optical Telescope Assembly (OTA) has slowed over time, and the model of the long-term secular trend supplied by the Telescopes Group includes a number of exponential terms. In 2014, the Telescopes Group concluded that this model had been underestimating the shrinkage and added an extra linear term of −1.55 microns per year that applies after March 29, 2011[1].

For observations taken between 1994 and early 2003, an older model of the orbital breathing based on the results of Hershey et al. (1998) is available; however, this does not attempt to correct for the longer term secular variations due to the telescope truss shrinkage or secondary mirror motions. Such offsets need to be estimated from focus monitor data for a particular epoch and manually added by the user; however, such data is not available for all time periods and we have not attempted to include these secular corrections for data covered by the Hershey model.

1.3 Expected Focus Offsets for STIS Filtered Apertures

The STIS filters are in the same aperture wheel as the slits and as such always close to a focus plane. Inserting a filter will lengthen the focus relative to a clear aperture by approximately $t\,(n-1)/n$, where t is the filter thickness, and n is the index of refraction. For most STIS modes, the pre-launch internal alignment was set to make the detectors confocal with each other when using the clear apertures. Exceptions are the NUV-MAMA imaging mode, MIRNUV, which is intended to be in focus with a filtered aperture but not with a clear aperture, and FUV-MAMA imaging for which two separate optical elements in the MSM are provided – MIRFUV for use with filters and MIRCUV for use with the clear aperture. However, for CCD imaging, only one optical element, MIRVIS, was provided.

[1] http://www.stsci.edu/hst/observatory/focus/FocusModel

For STIS the narrowband F28X50OII filter centered at 3738 Å with a FWHM of 57 Å is the most useful filter for phase retrieval. The pre-launch system engineering report SER STIS-CAL-018 (Ebbets 1995) specified that the narrowband F28X50OII filter has an index of refraction $n = 1.55$ and a thickness $t = 1$ mm. This should result in a shift of the best focus at the aperture plane between F28X50OII and 50CCD of about $t\ (n-1)/n = 0.355$ mm, which is equivalent to about 325 motor steps of the STIS corrector or a secondary mirror motion of about 3.23 microns. Focus offsets for other STIS filtered apertures and slits should be very similar. When quoting phase retrieval results for the STIS F28X50OII aperture in this report, we will *not* include any correction for this offset from the unfiltered 50CCD aperture.

STIS imaging filters are tilted by 3° relative to the optical path to offset any reflections away from the main image. Because of this tilt, refraction in the filter will also produce an offset of the image position relative to that in the clear filter. For the F28X50OII, SER STIS-CAL-018 calculated that this offset should be 1.337 pixels, which is very close to the offset of 1.314 pixels tabulated in the SIAF file for this filter. The SIAF file includes this offset in the filter aperture definitions, so when switching between a 50CCD and a F28X50OII image, *HST* is repointed to compensate for the refraction shift.

2 Small Aperture Throughputs

Flux calibration observations of standard stars generally use large apertures, 52X2 for 1st order models and 0.2X0.2 for echelle modes, to ensure photometric repeatability. GO observations often use smaller apertures to improve spectral purity; however, observations of a given target are rarely repeated. This makes it difficult to use most GO observations to check for anomalies in the STIS focus at the aperture plane. An exception is program 13346, "Advanced Spectral Library II; Hot Stars", which performed a number of echelle observations of O, B, and A stars using a variety of echelle CENWAVE and aperture combinations. These visits executed between August 2013 and January 2015. In this program, observations at a given setting were often deliberately broken into a number of shorter exposures both within an individual visit and across visits. Since most of the 13346 targets are not expected to be substantially variable and have well determined fluxes from previous observations, this program provides an opportunity to study variations in the small aperture throughput as a function of the modeled focus value. Since the particular grating/aperture combinations used were chosen primarily to adjust the count rates to be as high as possible without violating bright object limits, this does result in a rather heterogeneous set of observations.

In Figures 1 through 6, we show for select targets and CENWAVE/aperture combinations used in program 13346, the ratio of the flux as observed using the standard STIS pipeline calibration to the best available estimate for that target's intrinsic flux. For most of the targets observed, accurate flux estimates are available from IUE spectra, and were compared to the extracted fluxes measured in the observations. Nichols & Linsky (1996) and Bohlin et al. (2014) have argued that normalization of the IUE NEWSIPS flux calibration is low by 6% relative to the current HST flux calibration, and we have applied this correction to the published IUE fluxes used for reference. With this correction, the absolute flux scale for IUE

low dispersion large aperture observations should be accurate to within 5%, with somewhat larger errors for high dispersion large aperture IUE observations.

For the 13346 data, observations with small clear apertures such as the 0.2X0.06 or 0.2X0.09, which are recommended for good resolution with the echelle detectors, tend to show increasing throughput as the model focus becomes more negative. A few E230H exposures with the 0.2X0.09 aperture appear to show the throughput continuing to rise down to model focus values as small as −6 microns of equivalent secondary motion. Observations through small ND filters suggest a peak throughput near −4 microns. For filter thickness of 1 mm and an index of refraction near 1.5, this is approximately consistent with the expected 3.5-micron difference in the best focus. For the somewhat larger 0.2X0.2 aperture there is no apparent trend of the throughput as a function of focus.

In earlier cycles observations using the 0.2X0.09 or smaller apertures were most commonly done as either long ACCUM exposures that covered entire visibility periods or as single short exposures that were not repeated. These exposure strategies make it difficult to detect any throughput changes as a function of orbital breathing. However, program 8595 in 2001 observed the white dwarf standard stars GD 153 and HZ 43 for several orbits using the E230H 2513 0.2X0.09 combination while taking repeated exposures of 900 to 1000s duration. This provides sufficient time resolution and repeatability to usefully compare the aperture throughput in early 2001 to the 2013/2014 observations from program 13346 made using the same instrument configuration. This is shown in Figure 2. At both epochs, the throughput improves at more negative focus values, but the offset from zero of the estimated best focus of about −9 microns implied by the 2013/2014 data differs noticeably from the approximate −4 micron offset that best fits the 2001 data. This interpretation does come with a few caveats; the Hershey et al. (1998) focus model used for the 2001 data differs significantly from the Niemi & Lallo (2011) model applied to the later data, the adopted fluxes for the targets observed by program 13346 will not be as precise as those of the WD standards observed by 8595, and even under the best of circumstances substantial offsets of the actual focus from the model focus are possible. However, the 8595 observations were distributed in four separate visits spread over nearly 3 months, and the visit-to-visit consistency would argue against short-term deviations from the focus model having a substantial effect.

The heterogeneous nature of the 13346 data complicates the determination of trends, as there are multiple targets with uncertain absolute normalization observed with a wide variety of CENWAVE/aperture combinations. Repeated observations with the same target and configuration were often taken close together in time. A later multi-cycle GO program, 13841/14340 (PI Gallene), performed repeated observations of hot companions of two Cepheids at regular intervals between late 2015 and mid-2016 using the E140H 1234 setting with the 0.2X0.09 aperture. The exposures in these later programs were also done as orbit-long time-tag observations that allow the variation of the throughput as a function of orbital phase to be more finely sampled. At these short wavelengths, the hot companion rather than the variable Cepheid star should dominate the spectrum. Comparing the aperture throughput as a function of the model focus for these observations (Figs. 7 and 8), shows trends that are qualitatively similar to those seen from the 13346 data, with a tendency towards higher throughputs at

more negative model focus, although some individual visits deviate from the overall trend.

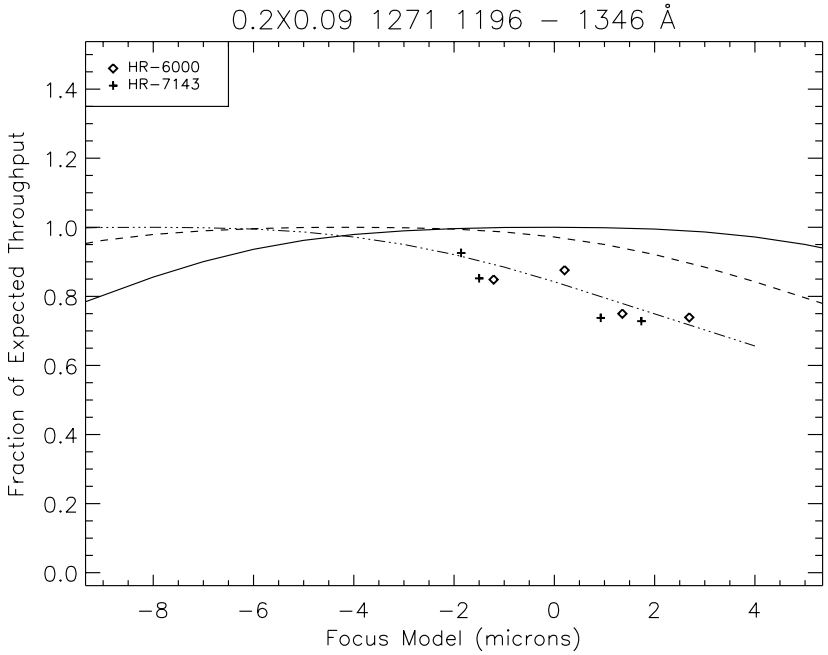

Figure 1: The symbols show the ratio of the measured to the expected count rate for observations taken during program 13346 using the 0.2X0.09 aperture, and the E140H 1271 CENWAVE setting. A different symbol is used for each target. The solid line shows the expected aperture throughput at this wavelength as a function of focus, calculated using the procedures discussed by Bohlin & Hartig (1998). The dashed and dotted curves show the same relation shifted by –4 and –8 microns, respectively.

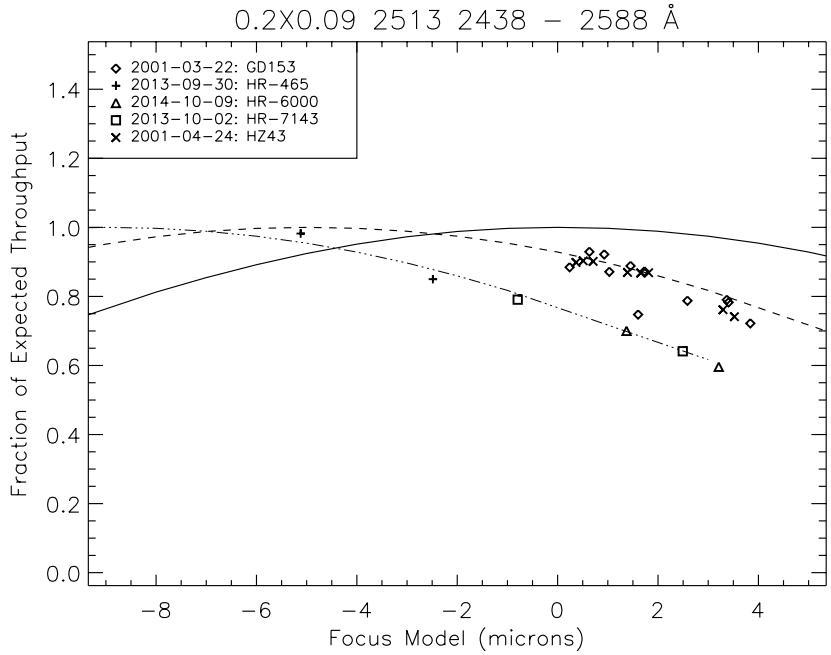

Figure 2: The same as the previous figure, except for observations using the 0.2X0.09 aperture with the E230H 2513 setting. For this grating and aperture

combination, there was a series of short ACCUM exposures of the WD standard stars HZ 43 and GD 153 taken in 2001 that provides a useful comparison to the observations from program 13346. In this figure the curves for the expected throughput as a function of focus are offset by 0 (solid), –5 (dashed), and –9 (dash-dot) microns.

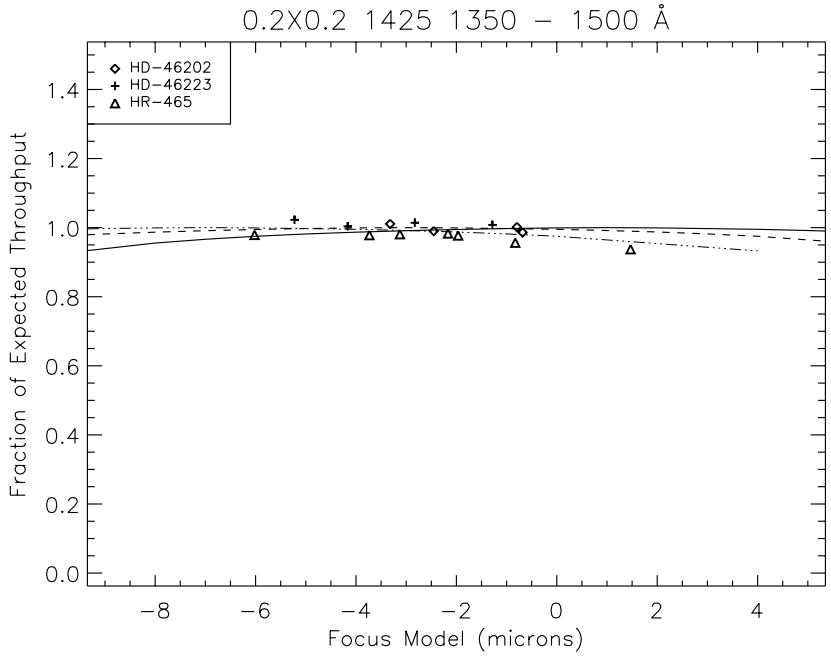

Figure 3: Symbols and lines are as Fig. 1, but here showing results for E140M 1425 observations with the 0.2X0.2 aperture. The solid, dashed and dash-dot curves show the model throughput as a function of focus for this aperture and wavelength shifted by 0, –4, and –8 microns, respectively.

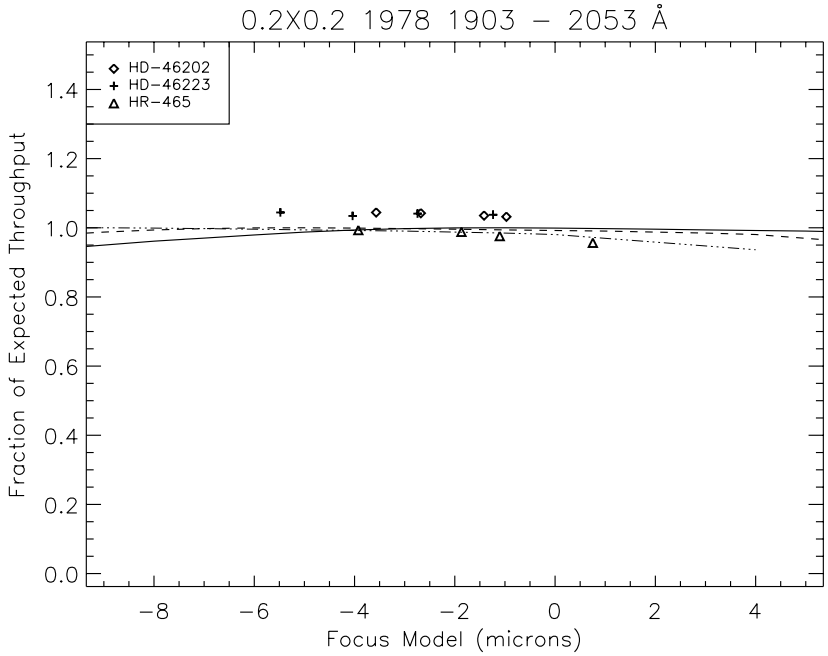

Figure 4: Symbols and lines are as Fig. 1, but here showing results for E230M 1978 observations with the 0.2X0.2 aperture.

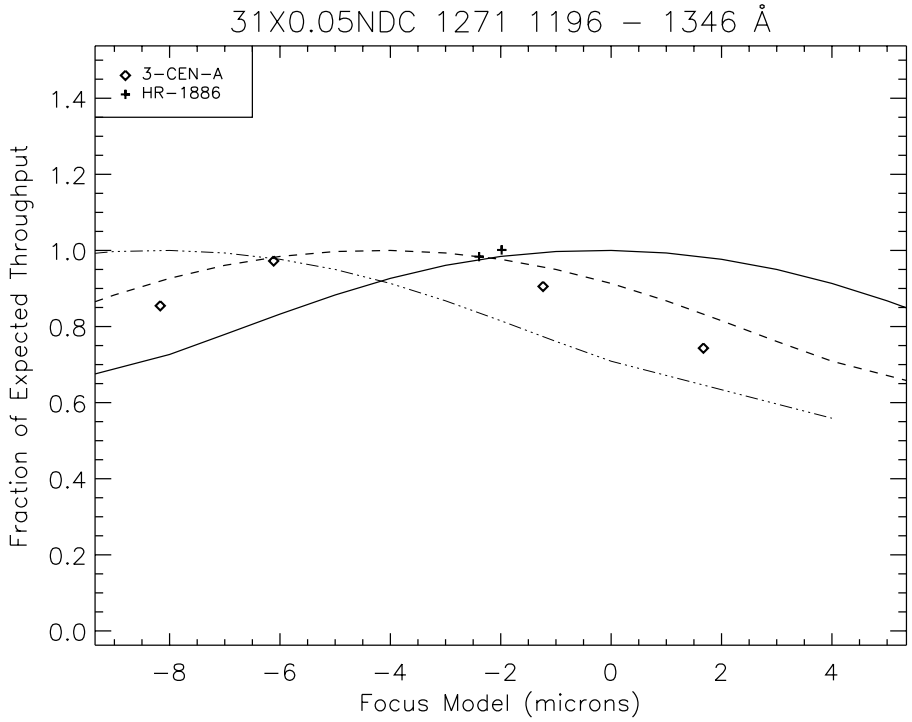

Figure 5: Symbols and lines are as Fig. 1, but here showing results for E140H 1271 observations with the 31X0.05NDC aperture.

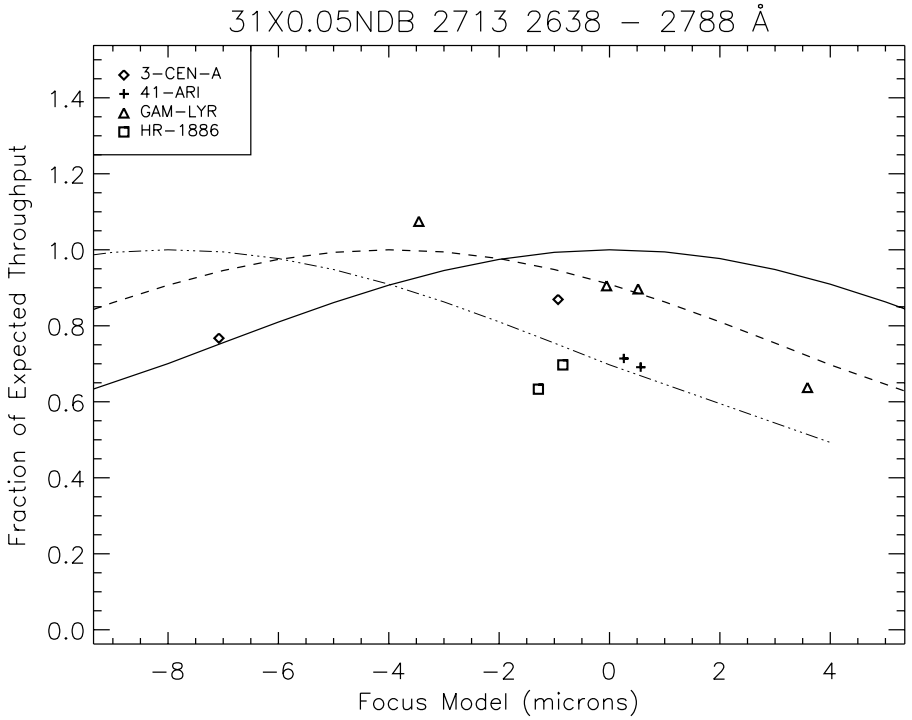

Figure 6: Symbols and lines are as Fig. 1, but here showing results for E230H 2713 observations with the 31X0.05NDB aperture.

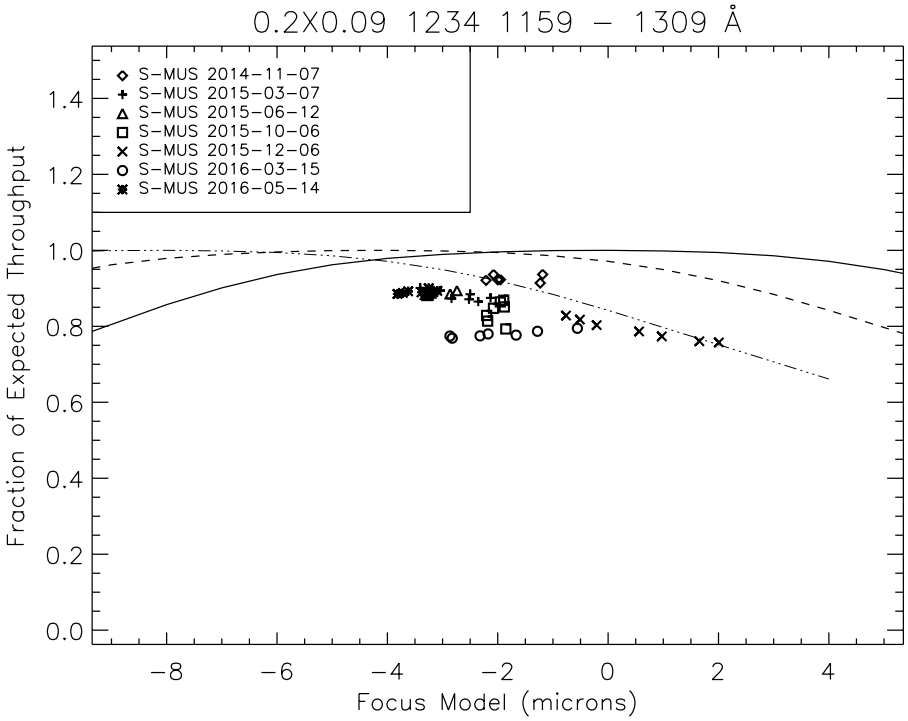

Figure 7: This figure is similar to Fig. 1, except that here we plot the relative throughput as a function of the model focus for each 300 s subset of each one-orbit time-tag exposure from the recent GO programs 13841 and 14340 which have been repeatedly monitoring the same stars. Different symbol types are used to distinguish the individual visits. While these targets are Cepheid variables, the FUV flux in each case is dominated by a blue companion and is not expected to vary significantly as the Cepheid pulsates. Here we show results for the target S Mus observed using the E140H 1234 setting with the 0.2X0.09 aperture.

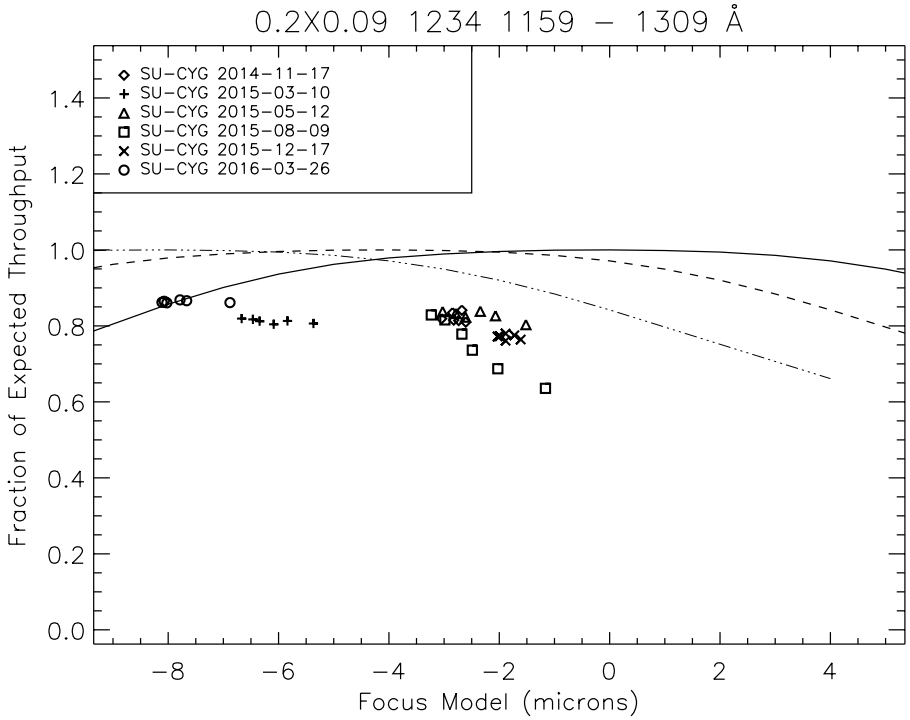

Figure 8: As in Fig. 7, expect for the target SU Cyg.

3 OII phase retrieval

The sparse and heterogeneous nature of the small aperture throughput measurements make it difficult to track relative focus changes over time, and so we now turn to estimates of the focus based on phase retrieval of narrow band images.

3.1 The STIS F28X50OII filter and Phase Retrieval

We performed phase retrieval for STIS OII images using the procedures originally developed by Krist & Burrows (1995). These procedures fit PSF models to the image allowing a number of the Zernike coefficients to vary. In our fits we simultaneously solved for the Z4 (focus), Z5 (zero-degree astigmatism), Z6 (45-degree astigmatism), Z7 (x-coma), and Z8 (y-coma) Zernike terms. We also assumed that the ratio between the Zernike focus coefficient, Z_4, and the equivalent secondary mirror motion is given by $Z_4/dsM = 0.0061$ (Lallo et al. 2005). Unfortunately, the procedure of Krist & Burrows does not include any formal estimate of the errors in the fitted coefficients. This makes it difficult to judge how the errors scale with the S/N of the observation and when a given star is too faint to give reliable results.

3.2 OII imaging exposures over time

The F28X50OII filter is most frequently used for target acquisition, and only a limited number of ACCUM mode images suitable for phase retrieval were taken for calibration or science purposes. As discussed above, at optimal focus value for STIS 50CCD clear aperture imaging, we would expect phase retrieval for F28X50OII images to show a focus offset equivalent to about -3.23 microns of HST secondary offset. However, when discussing OII filter results, we will not correct the value obtained from the phase retrieval for this expected offset, and will simply quote the OII focus measurements rather than the inferred focus value for a clear aperture.

ACCUM OII Images

There are a limited number of F28X50OII images taken in ACCUM mode that are suitable for phase retrieval. Results for these images are shown in Figure 9, where we subtracted the predictions of the Niemi & Lallo or Hershey focus model from the directly measured phase retrieval value for the OII filter. During the pre-SM4 period covered by this model, the mean offset between the OII ACCUM phase retrieval results and the model was −6.45 microns. For the data taken after SMOV4 in 2009, the mean offset from the focus model was −6.59 microns. For the deep images taken in 2015 and 2016 as part of programs 14063 and 14425, the mean offset from the model was −1.57 microns, a change of about +4.2 microns from either the pre-SM4 or the 2009 values. If we assign an error of 1.5 microns to each OII ACCUM phase retrieval measurement, a linear fit to the data taken after March 29, 2013 yields a slope of +1.25±0.15 microns/yr.

As discussed above, the Telescopes Group has added an extra linear term to the secular focus model of −1.55 microns per year that applies after March 29, 2013. To best fit the STIS OII ACCUM measurements a much smaller extra secular term of only −0.3±0.15 microns/year would be needed.

ACQ OII Images

The F28X50OII filter is often used for acquisitions of bright stars. This results in two images of the external target that are available for subsequent analysis. The 1st image is taken at the initial telescope pointing, while the second is taken after the initial coarse locate phase, which should have moved the target image to a standard reference position on the detector. The final fine-locate phase then moves the target to align with the lamp image of the standard 0.2X0.2 aperture, but no image of the target is taken at the final pointing.

Over 640 STIS ACQ exposures have been taken with the F28X50OII aperture. This potentially provides a much larger number of independent focus measurements than is possible with ACCUM images. In addition, these images have the advantage that the target should almost always be well centered on the detector. However, there are a few caveats that apply to these data. Each of the two ACQ images downlinked to the ground are actually created on-board the spacecraft from a pair of dithered images that are combined by shifting them into alignment and taking the minimum value at each location. This provides robust rejection of cosmic rays and hot pixels, but will also bias the statistics of the image, especially if the S/N is low or for cases where the dither does not properly align the images. Phase retrieval measurements in particular are very sensitive to the relative brightness of the peak pixel relative to the wings. If the on-orbit processing preferentially suppresses the wings due to the larger fractional noise there, this could result in phase retrieval estimates closer to zero focus offset than is appropriate.

We applied a slightly modified version of the standard phase retrieval script to the second image in each STIS F28X50OII acquisition exposure, which is taken after the fine locate phase has moved the target to a standard position on the detector, but before the target has been shifted to align with a lamp image taken through the 0.2X0.2 aperture. We discard those cases where the estimated S/N is less than 25, where the peak pixel may be saturated, or where the target is not well centered in the subarray. After this screening, 579 ACQ exposures remain, covering the time span from May 3, 1997 to May 14, 2016.

For data taken since March 2013, the results show a slope very similar to that seen from the ACCUM data sets (Fig. 10). There is, however, a tendency for the ACQ results, especially at earlier times, to be offset closer to zero focus compared to the ACCUM results from similar periods, with average values close to −5 microns for most periods prior to 2011, rather than the approximately −6.5 microns average offset found from the ACCUM OII images.

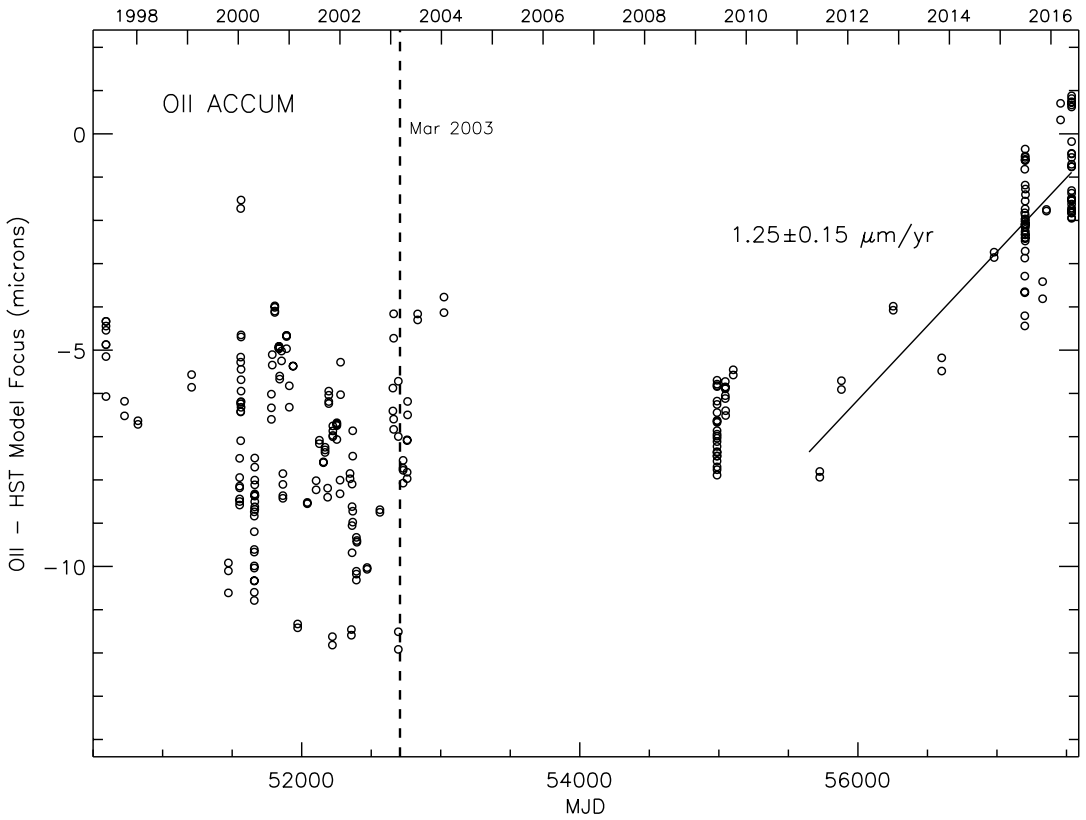

Figure 9: For observations subsequent to March 3, 2003 we plot the offset between the focus as measured from phase retrieval of STIS OII ACCUM images and the Telescopes Group focus model. We do not include here any correction for the offset expected between the filtered F28X50OII and the clear 50CCD. For observations before that date, we correct the raw phase retrieval results using the older Hershey breathing model, but do not include any other secular corrections. Also shown is a linear fit to the offset between the OII and model values for the period after March 29, 2011, the time after which the Telescopes Group added an extra -1.55 microns per year of OTA shrinkage to the secular model.

Other Aberrations from OII images

The fitting for the F28X50OII focus also solves for coma and astigmatism values, (Zernike coefficients Z7 and Z8 for the coma, and Z5 and Z6 for the asigmatism). The values for these other abberations as measured over time are shown in Figure 11 for STIS ACCUM OII images and in Figure 12 for ACQ images. There is a suggestion of a systematic change in the X-COMA value over time. Fitting the ACCUM data and adopting the scatter about a linear fit as an estimate of the error results in the relation X-COMA = –0.00196 ± 0.00046 – (0.000485 ± 0.000041) × (year – 1997.395) (rms microns), where the value of the slope is about 11 times its estimated error. Trends for the other abberation coefficients are weaker, with less than about 3 sigma significance, and may be affected by the systematic differences in the measurements over time. Results from the ACQ images show a slightly larger slope for the X-COMA of 0.000764 ± 0.000077 rms microns/year. While these changes may suggest a change in the optical alignment over time they do not appear to correlate with the change in throughput or focus that appear to have occurred subsequent to 2011.

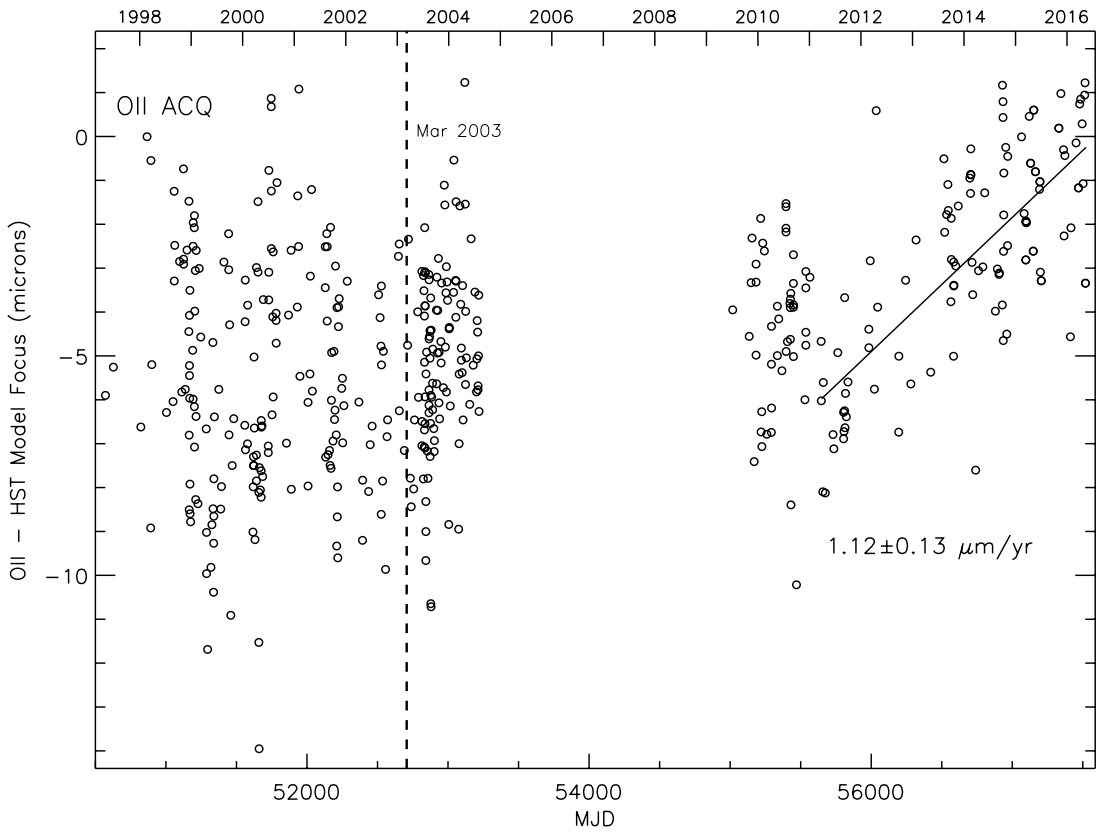

Figure 10: As Fig. 9, except here we plot the results for deep OII ACQ images taken near the center of the STIS CCD detector.

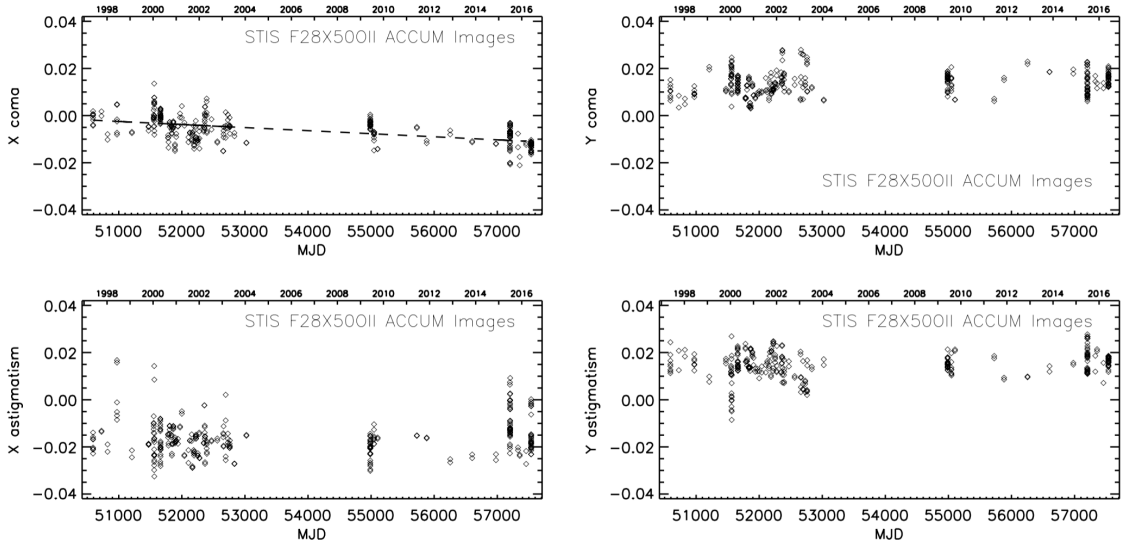

Figure 11: Values for coma and astigmatism as measured from the STIS OII ACCUM images used for the focus evaluation. The dashed line in the first panel shows the best linear fit to the X-coma as a function of time.

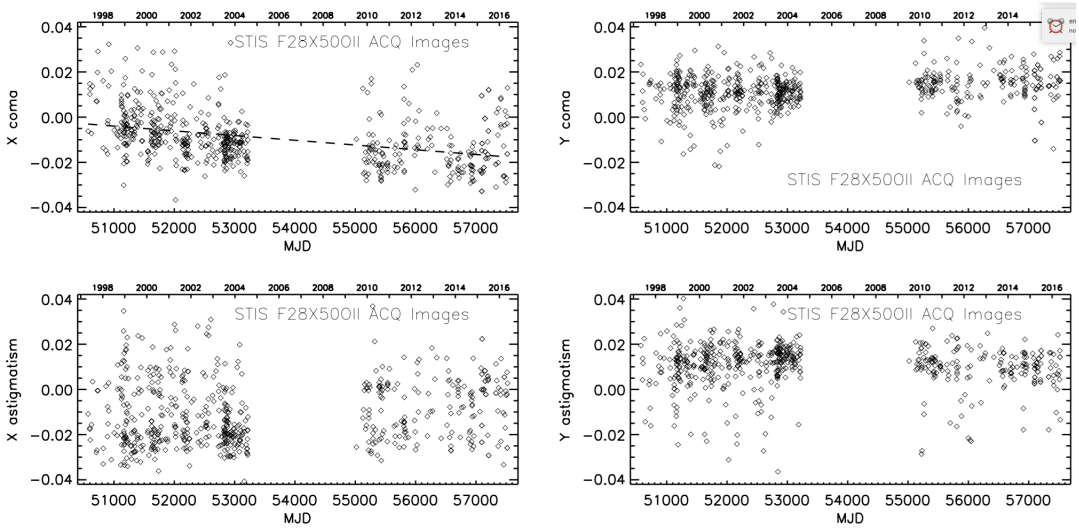

Figure 12: Values for coma and astigmatism as measured from the STIS OII ACQ images used for the focus evaluation.

3.3 OII images in parallel with other HST Cameras

Contemporaneous observations from 2000

Lallo (private communication), compared 5 visits of STIS OII images taken along with parallel WFPC2 phase retrieval images in 2000 as part of program 8829, and concluded that the mean offset of the focus measured from those STIS OII images from the best PC focus was –7.2±0.44 microns. This is only slightly larger than the mean pre-SM4 offset of –6.45 microns we estimated from the phase retrieval of the OII ACCUM images discussed above (Fig. 9).

Parallel observations from 2015/2016

To confirm the size of the focus offset suggested by the OII images, parallel observations with STIS-CCD/OII, WFC3-UVIS/F410M, and ACS-WFC/F502N were undertaken. The telescope pointing was selected to put a UV bright star at the center of the STIS CCD detector that would give > 35,000 e- in the peak pixel, while parallel exposures were taken with the WFC3 F410M with the goal of having a number of stars suitable for phase retrieval included in the WFC3 frame. Two fields, one in NGC 188 and one near 47 Tuc were observed in June 2015 as part of program 14063. The 47 Tuc field was observed again in May 2016 in program 14425. In the denser 47 Tuc fields, there are several tens of stars available in each WFC3 image for the phase retrieval and these results should be the most reliable. The density of suitable stars in the NGC 188 fields is much lower than in the 47 Tuc fields.

To sub-sample the PSF and avoid the possibility of all the STIS exposures being affected by a poorly placed hot pixel, a four-position box dither was used with 5.5 pixel spacing. At each of these dither positions two 290s OII exposures were taken for the NGC 188 target, and six to eight 20 to 35s exposures for the brighter 47 Tuc target. At each position, either a single WFC3-UVIS exposure or both a WFC-UVIS and an ACS-WFC exposure were also taken in parallel. The time needed for dumping the instrument data buffers made it impossible to take four full frame images with both the WFC3-UVIS and the ACS-WFC in a single orbit. For the 47 Tuc field, two full-frame ACS-WFC images were taken together with the first and last of the four

full-frame WFC3-UVIS exposures, while for NGC 188 an ACS-WFC2-2K sub-array exposure was taken with each of the four full-frame WFC3-UVIS images.

Observations of the 47 Tuc field were repeated in May 2016 in program 14425. These OII measurements were already included in Figure 9 where they were compared with the focus model. Here we compare them directly to the parallel phase retrieval results for ACS and WFC3, which should remove any uncertainties associated with the focus model.

The ACS subarray images of NGC 188 were processed with a custom subarray bias frame obtained during the visit. All other images were processed with the standard archive calibration pipelines. The FLT images were analyzed using standard phase retrieval scripts and initial Zernike coefficients included in the Appendix. For the NGC 188 fields, 10 stars were measured on WFC3 and 6 stars on ACS. These values were adjusted for the tabulated chip-to-chip offsets included in Table 1 and are plotted in Figure 13. For the denser 47 Tuc fields, 11 stars were measured in ACS images. The stars in the WFC3 images were bright enough (~25000 to ~35000 electrons) and isolated enough to be included in a PSF library under development by Jay Anderson. Use of this library aids with consistent identification and characterization of the detected sources. Stricter isolation criteria were applied to exclude PSFs with phase retrieval fits affected by contaminating flux from neighbors, and a few remaining anomalous focus fits were rejected. The number of stars used after this selection then ranged from 55 to 74 on UVIS1 and 70 to 101 on UVIS2, with similar numbers for the observations made in 2015 and 2016. These results are shown in Figures 14 and 15.

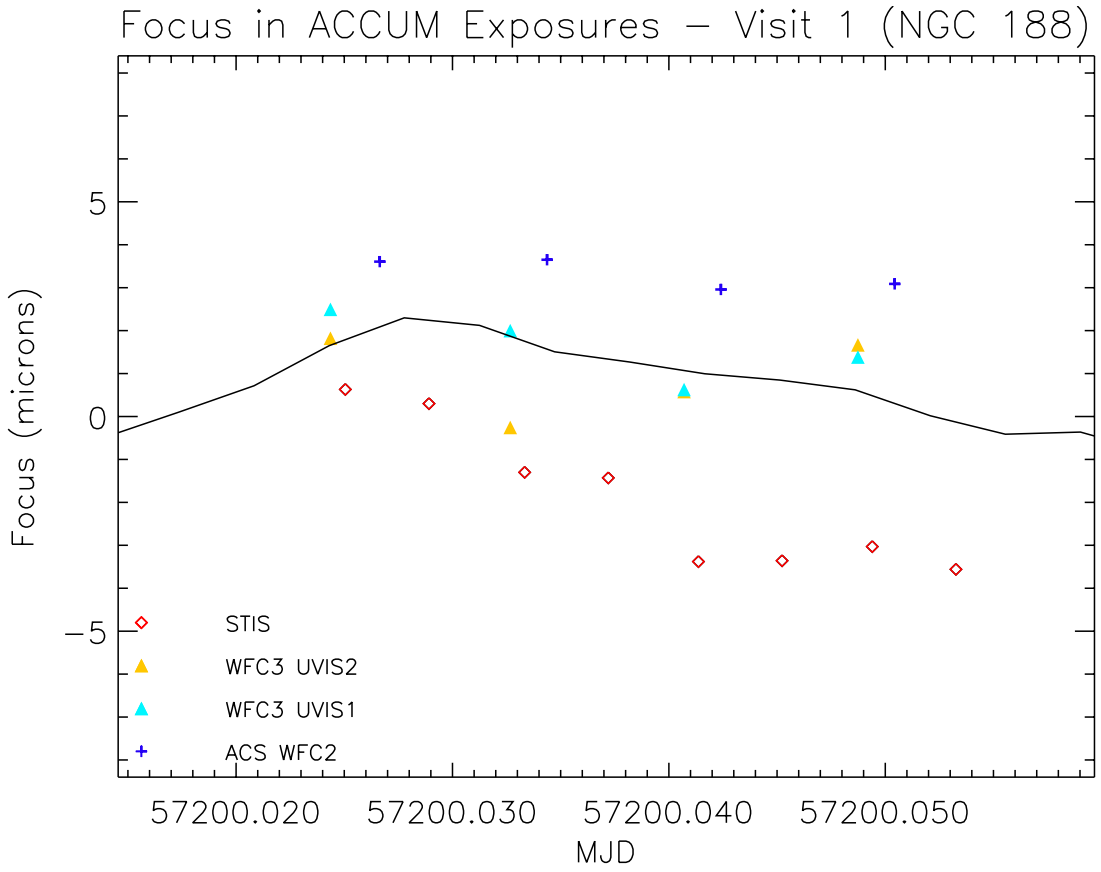

Figure 13: Average phase retrieval results for each detector are compared to the tabulated focus model (solid line) for the June 2015 parallel images taken of NGC 188 with WFC3 UVIS F410M, ACS WFC F502N, and STIS CCD F28X50OII. For ACS and WFC3 the detector offsets tabulated by Cox & Niemi (2011) were subtracted from the measured focus values. This correction noticeably reduced the offset between the different chips, especially for the WFC3 UVIS1 and UVIS2. Note that the STIS OII filter shifts the focus relative to the clear STIS aperture by -3.23 µm. That is, if we corrected the results to give the estimated focus for the 50CCD rather than the OII aperture, the STIS data points in this and subsequent figures would shift upwards by 3.23 µm.

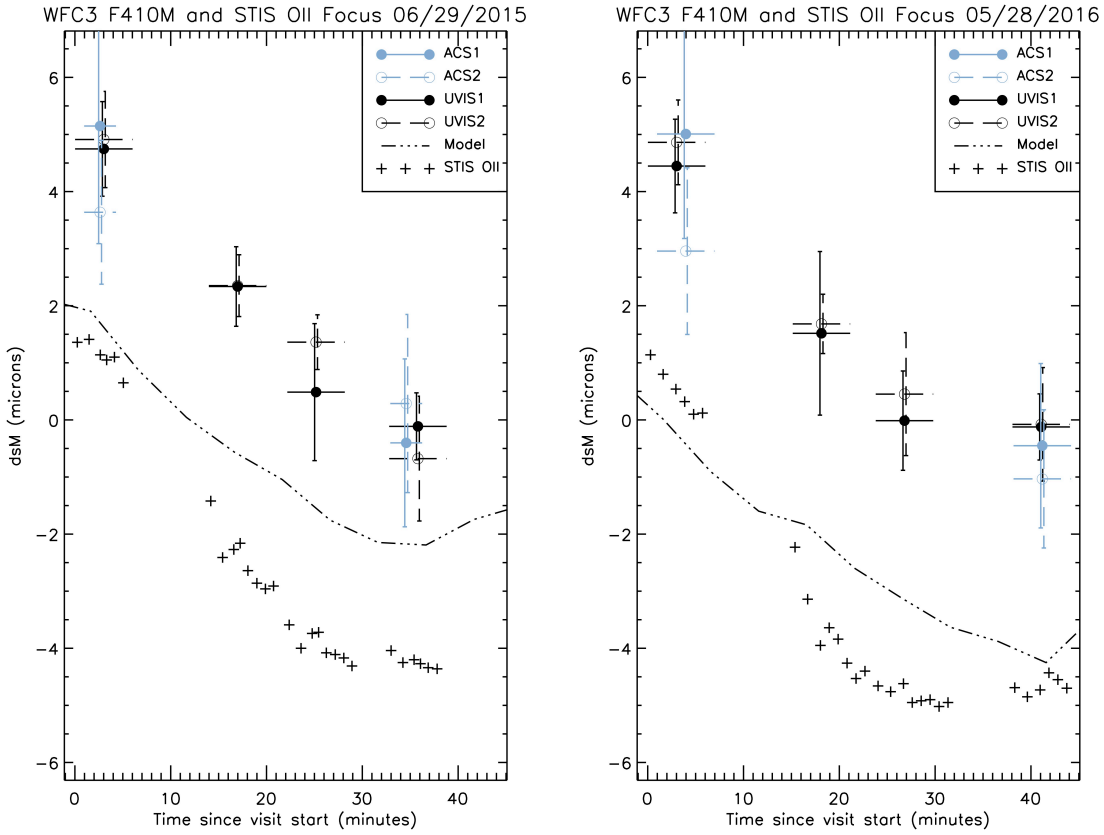

Figure 14: Measured focus values for observations in the field of 47 Tuc performed on 29 June 2015 (visit P2 of program 14063) and 28 May 2016 (program 14425) are shown. For each ACS and WFC3 exposure, the median focus value derived for stars measured on each chip were corrected for the expected focus offset for that chip. The vertical bars over-plotted on the WFC3 and ACS exposures show the RMS scatter of the measurements, while the horizontal error bar shows the length of each exposure. The points shown for STIS display the individual focus measurements made using the bright star HD 2072 which was observed with the F28X50OII filter near the center of the STIS CCD detector; for these measurements no correction for any expected offset was applied. The dash-dot line shows the predicted HST focus model for the period supplied by the STScI TEL Group.

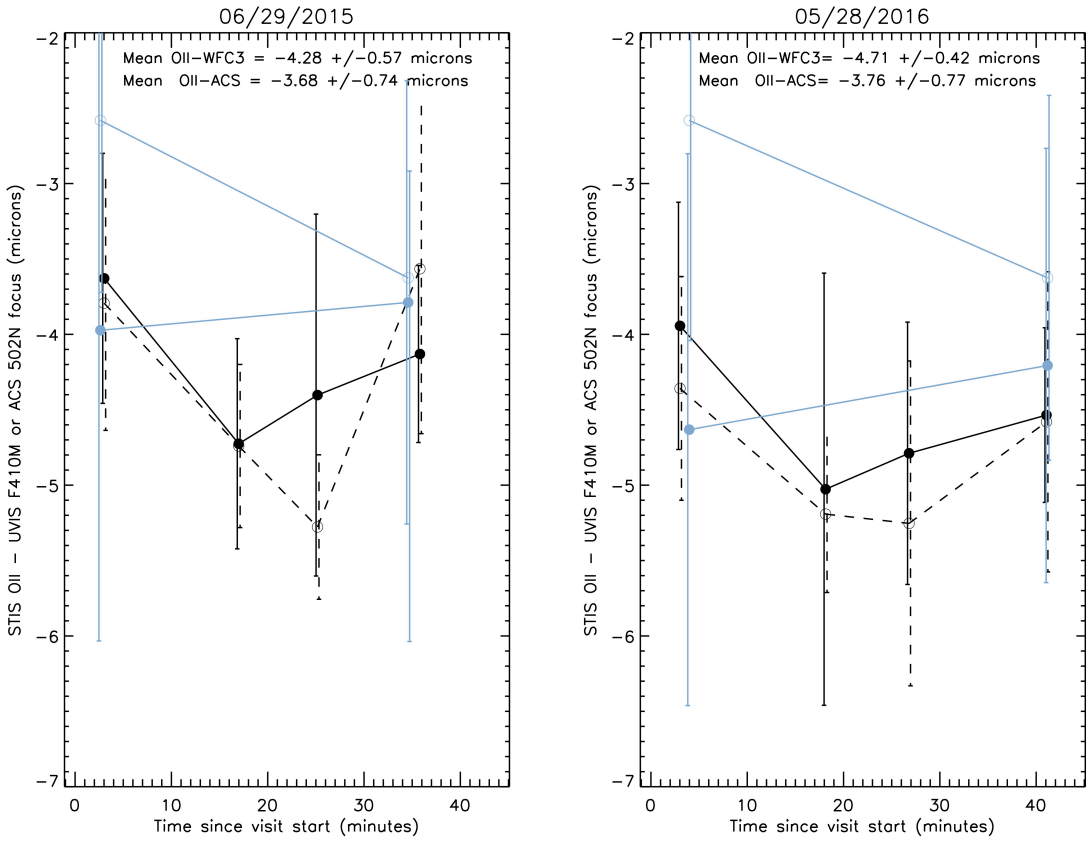

Figure 15: The focus value for each of the ACS and WFC3 exposures shown in Fig. 12 is subtracted from the mean focus value of the overlapping STIS observations to provide direct measurements of the STIS OII – mean observatory focus offset independent of the adopted telescope breathing model. The vertical "error" bars shown here are defined in the same way as in Fig. 14.

Table 1: The offset between the mean focus measured from the STIS OII images and the parallel WFC3/UVIS and ACS/WFC3 images. The WFC3 and ACS focus values have been corrected for the measured offset of each detector from the observatory mean (Cox & Niemi 2011). **The quoted errors are calculated by dividing the RMS scatter of the individual offsets by the square root of the number of measurements and should be considered a lower limit to the true error.**

	Applied offset	NGC 188	47 Tuc	47 Tuc
	(microns)	27-06-2015	29-06-2015	28-05-2016
STIS OII – ACS WFC2	+0.303	-5.18	-3.47+/-0.58	-3.10+/-0.30
STIS OII – ACS WFC1	+0.832	No data	-3.88+/-0.05	-4.42+/-0.12
STIS OII – WFC3 UVIS2	+0.648	-2.70	-4.34+/-0.31	-4.85+/-0.17
STIS OII – WFC3 UVIS1	-0.487	-3.35	-4.22+/-0.18	-4.57+/-0.18
STIS OII – Focus Model	0	-3.10+/-0.43	-1.77+/-0.14	-0.86+/-0.19
<WFC3> – <ACS>	N/A	+2.15	+0.05	+0.66

Offsets measured for each detector are summarized in Table 1. The mean of all of the offsets from the 2015 visits is −3.74 microns, while the mean offset from the WFC3 results is −4.23 microns, and should be considered the most reliable. Although the absolute OII offsets estimated from comparison with the parallel images are 1 to 2 microns more negative than compared to the focus model, the absolute change with

respect to the Lallo et al. (2002) results still suggests a change of +3 microns over the last few years. Over the 11 months between the two 47 Tuc visits, the measured STIS focus decreased by an average of −0.43 microns with respect to WFC3 and −0.08 microns with respect to ACS, but *increased* by +0.91 microns relative to the observatory focus model. We suspect that the extra OTA shrinkage of −1.55 microns per year that the observatory model includes after March 2011 appears to have ceased and the continued inclusion of this trend in the model now causes it to be increasingly out of sync with the actual telescope.

Given the scatter and systematic uncertainties in all of the focus measurements, we see little evidence that the STIS focus relative to ACS and WFC3 changed between the two sets of 47 Tuc exposures. However, this offset does appear to be different from that estimated for earlier epochs, and we conclude that the relative 3.0±0.5 micron shift seen in the OII images over time appears to be confirmed by the direct comparison of phase retrieval results when the detectors are used in parallel. Since the images are taken simultaneously, this removes uncertainties related to modeling the breathing as well as any assumptions about the long-term secular trends in the focus. This also appears to be consistent with the approximately 4 micron change implied by the comparison of small aperture throughputs shown in Fig. 2.

4 Autocorrelation Analyses

Auto-correlation techniques offer a powerful tool for estimating the relative focus of different observations; as for a given intrinsic spectrum the width of the auto-correlation function should be at its minimum at best focus. This technique was used extensively during the focusing of the COS spectroscopic modes (Lennon et al 2010). For STIS this technique can potentially be used to check both the internal alignment using wavecal lamp exposures through small slits, as well as to study focus changes in external targets. However, the latter application requires repeated observations using the same configuration of very narrow-lined sources through relatively large apertures.

4.1 Internal Lamp Autocorrelations

Autocorrelation of deep wavecal lamp exposures taken using small apertures can be used to check for any changes in the internal focus of the instrument. Due to changes in the monitoring observations only a few modes have large numbers of suitable deep images spanning the history of STIS. The modes we have examined in detail are listed in Table 2. We find no consistent signature of increasing line autocorrelation widths over time. Nor is there evidence for any correlation with the telescope breathing model. Examples of autocorrelation results over time are shown below in Figure 16. We conclude that the relative focus of the STIS aperture plane and the STIS detectors has not systematically changed over the instrument's lifetime. This implies that any focus change for the STIS instrument with respect to the mean observatory focus would need to be due to an offset of the either the entire instrument or the corrector optics rather than an offset of the aperture plane or mode select mechanism (MSM) with respect to the detectors.

Table 2: Selected Settings with Deep Wavecals Suitable for Autocorrelation Analysis

Grating	CENWAVE	Aperture	Number	Median texp (s)
E230M	1978	0.2X0.06	17	87
E230M	2707	0.2X0.06	18	190
E140H	1271	0.2X0.09	20	400
E140H	1598	0.2X0.09	20	400
G230MB	2697	52X0.005	91	20

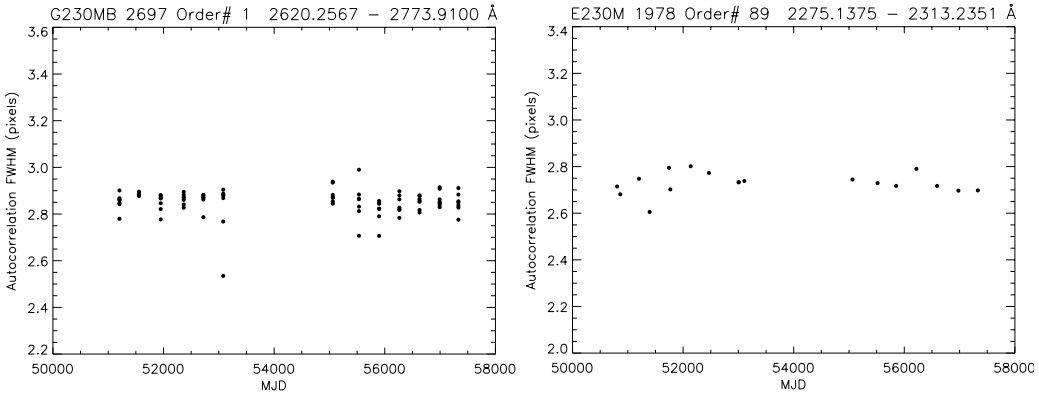

Figure 16: The FWHM of the autocorrelation function over time as measured from internal LINE lamp calibration exposures with the STIS CCD G230MB 2697 setting taken through the 52X0.05 aperture (left), and order 89 of the E230M 1978 setting with the 0.2X0.06 aperture. There is no evidence for any systematic change in the internal instrument alignment over time.

4.2 External Target Autocorrelations

Repeated observations of a narrow-lined external target at a variety of focus positions can also be used to find the best resolution. In practice looking for the minimum of the auto-correlation function width for a spectrum with many sharp features has proven to be significantly more robust than direct measurement of the profiles of a small number of narrow lines (Lennon et al 2010). However, this requires repeated and relatively short observations of a suitable target with the exposures well distributed over a range of telescope focus values. For this purpose exposures should also be done using aperture openings large enough that pointing or focus changes do not significantly truncate the PSF. Relatively few external STIS observations meet these requirements.

4.2.1 Autocorrelation of First Order CCD Spectra

A few of the more extensive campaigns to observe transiting extra-solar planets best fulfill these criteria. Figures 17 through 21 show a number of examples using 1st order CCD modes. Figures 17 and 18 appear to suggest that the G430L mode was close to optimal focus in 2003, and offset from optimal focus by perhaps one micron in 2009/2010 and perhaps slightly more in 2012. Unfortunately, there are not equivalent examples with this grating that sample a wide range of focus values at later times when the OII phase retrieval results suggest larger changes in the STIS focus.

There are a number of examples with the G750M 6094 setting (Figs. 19 through 21) well distributed over the 2009 to 2016 period, and these serve to illustrate both the power and the limitations of autocorrelation studies with archival data. In Figure 19 we see that the visit observing HD 189733 in early October 2010 implies a best focus several microns more positive than the visits of either November 2009 or November 2010. The lack of comparable offsets in the internal lamp auto-correlation results makes it unlikely that this is an internal alignment issue, and since the same patterns repeat from orbit-to-orbit within each visit it cannot be due to changes in the target spectrum. Examination of the attitude history and breathing model during and before the October 2010, visit shows that HST had spent an extended period of time at a sun angle of 54° before slewing to a sun angle near 112° for these observations. During the several hours preceding these observations, the focus model transitioned from an average focus near −4 microns to an average near +2 microns. If the actual focus was lagging behind the model focus during this period it would explain the offset seen in Figure 19. When *HST* is in a thermal state different from the examples used to define the breathing model, it would not be surprising to find that an offset between the actual and model focus persists for several hours. This makes it unwise to rely too heavily on comparison between any focus measurements and the focus model from one or a small number of visits.

Comparing the trends in Figures 19 through 21 for the G750M 6094 setting does suggest an evolution of the minimum in the autocorrelation function towards more negative values over time, although the considerable scatter combined with the small number of independent visits makes this difficult to quantify. Qualitatively, the 2009-2010 observations of HD189773 show best focus values ranging between about +0.5 and +3.5 microns of model focus, the 2013-2014 observations of α Cen between about -2 and 0 microns, while the 2015-2016 observations of HD 219134 find the best resolution between about -1 and < -3 microns.

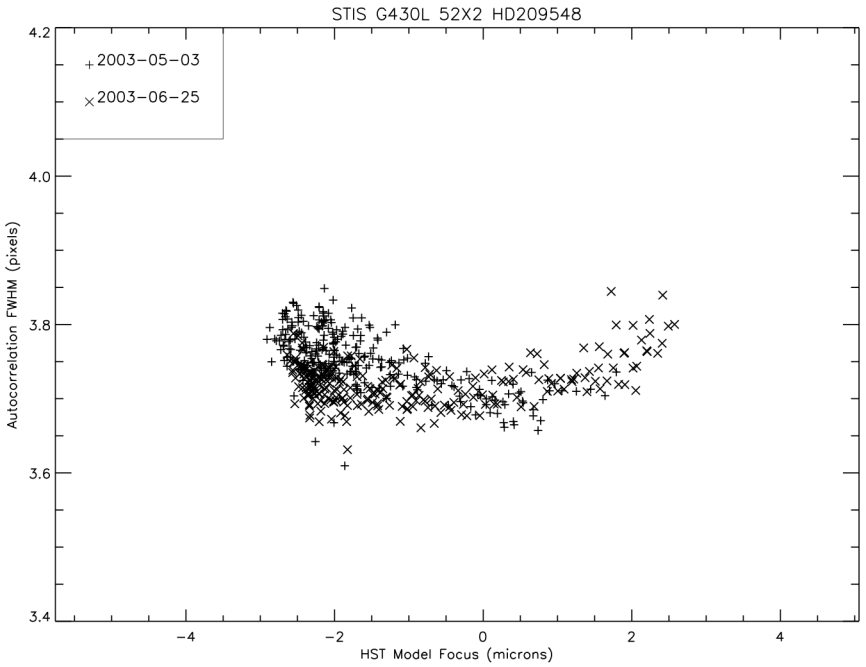

Figure 17: The autocorrelation function FWHM is plotted as a function of focus value for G430L observations of HD 209458 taken in 2003 as part of proposal 9447. The best resolution for these observations appears to be close to zero model focus.

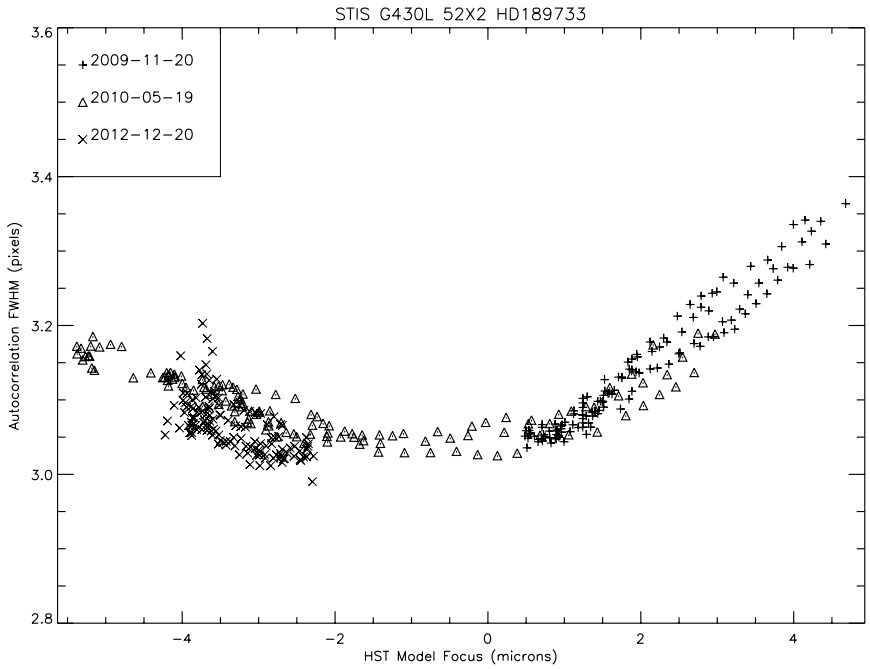

Figure 18: The autocorrelation function FWHM is plotted as a function of focus value for G430L observations of HD 189733 taken between 2009 and 2012 taken during programs 11740 and 13006.

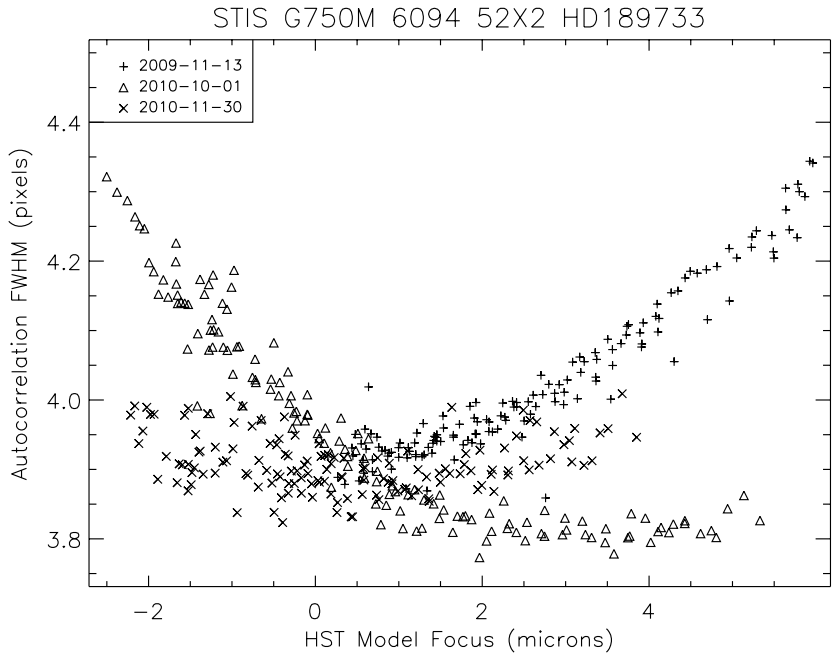

Figure 19: The autocorrelation width as a function of model focus for observations from program 11572, which targeted HD 189733 with the G750M 6094 setting, is shown. Results from the October 2010 visit are very different from the visits that occurred 11 months before or 1 month after.

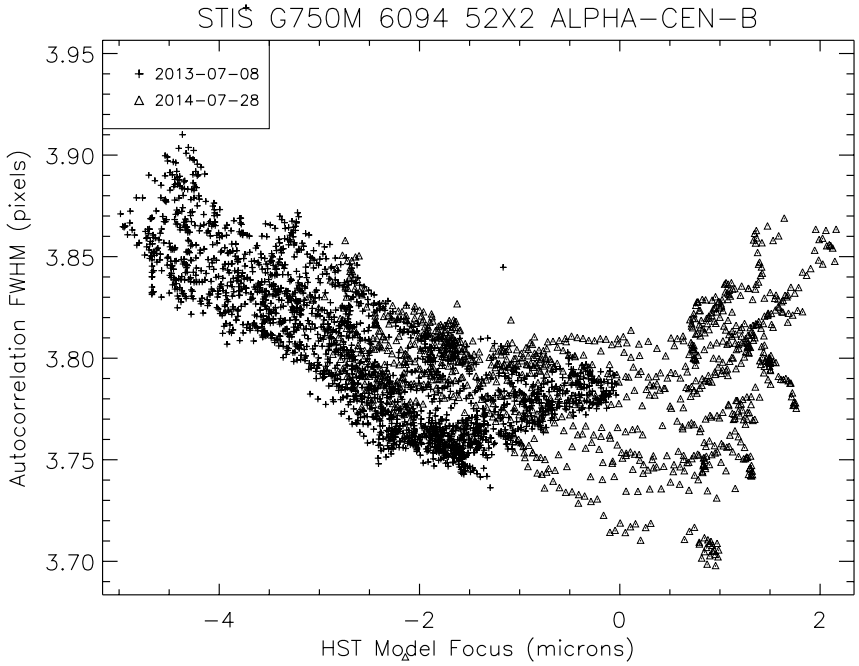

Figure 20: The autocorrelation width as a function of model focus from observing programs 13180 and 13927, which targeted α Cen B with the G750M 6094 setting.

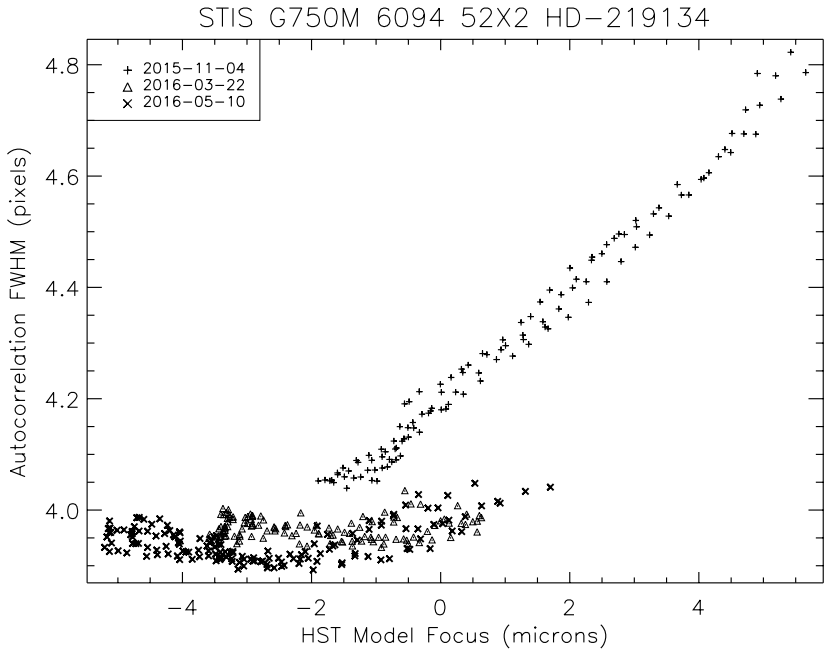

Figure 21: The autocorrelation width as a function of model focus for three visits of program 13665, which observed HD 219134 with the G750M 6094 setting.

4.2.2 MAMA Echelle Autocorrelation

For MAMA modes, there are far fewer good examples suitable for autocorrelation analysis, as it is uncommon to take multiple short observations of the same object when substantial spectral variability is not expected. E230M observations of the

transiting plant HD 209458 were taken over three visits in 2010, as shown in Fig. 22. The autocorrelation results appear to show improved focus at negative model focus offsets, suggesting that there was a substantial offset at that time in the best focus of the E230M mode from the CCD first order modes discussed above.

Few other STIS echelle observations have obtained repeated observations of sufficiently stable and narrow lined stars to provide a good test of the autocorrelation width as a function of focus. In Figure 23, we show results for observations of the narrow lined star HR 465 in the fall of 2013 as part of program 13346. As there are only a handful of separate observations, we show results for a number of echelle orders on the same figure. The E140M observations showed no evidence for improved focus at negative model focus values, while E230M observations of the same target do support at least a modest offset towards negative focus, similar to that seen for HD 209248.

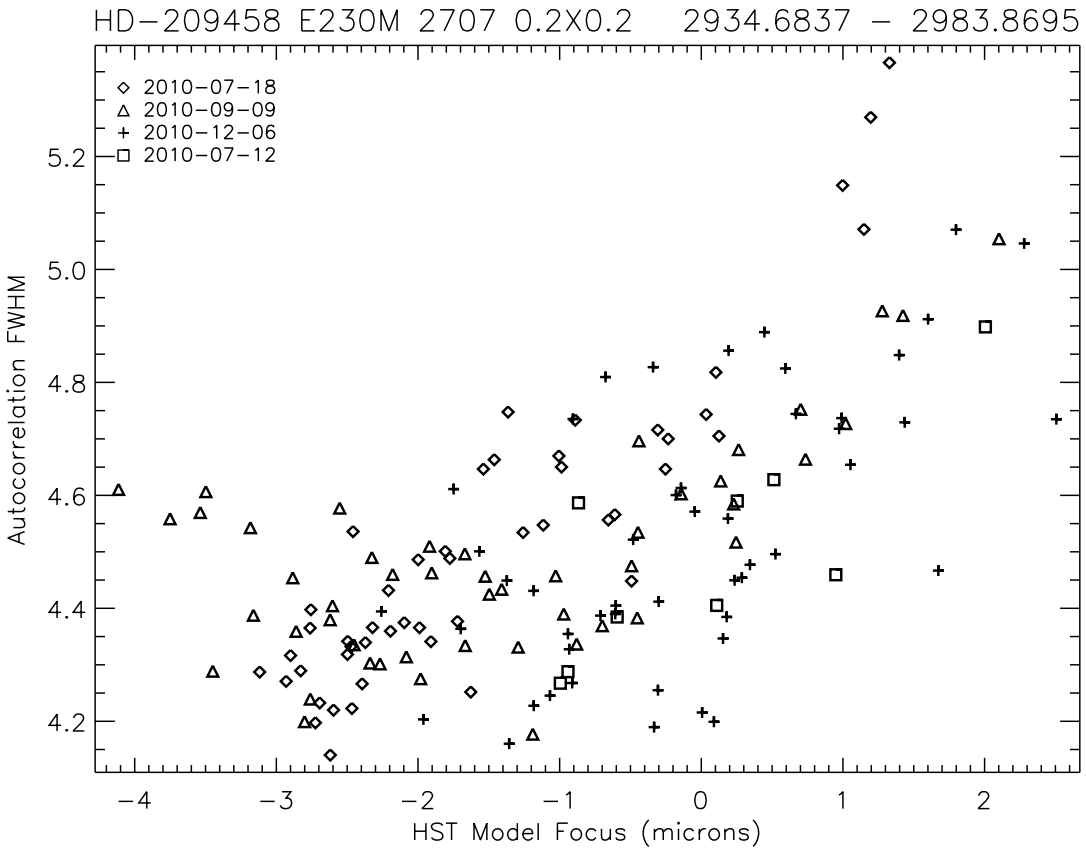

Figure 22: Observations of HD 209458 taken between July and December 2010 during proposal 11576 suggest noticeably better resolution at model focus values at or below -3 microns. Results are shown here for only echelle spectral order 69, although very similar correlations can be seen in many other orders of this set of observations.

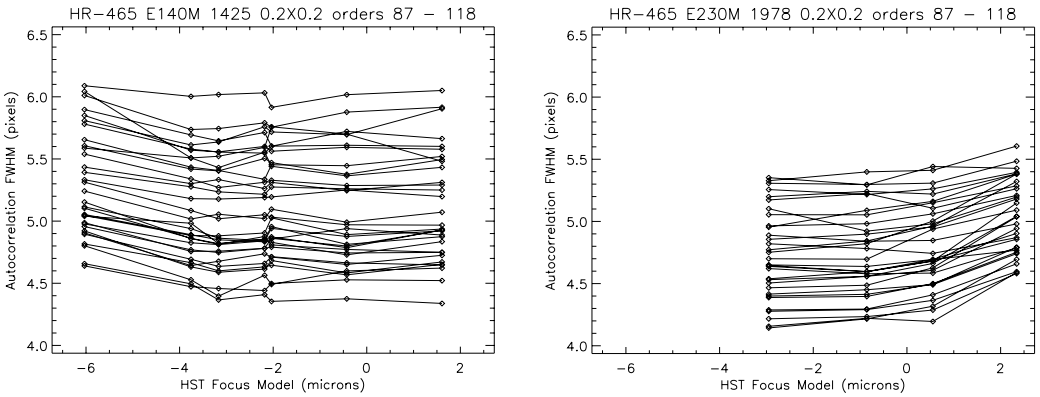

Figure 23: Autocorrelation results are shown for a number of individual spectral orders for E140M (left) and E230M 1978 (right) 0.2X0.2 observations of the narrow-lined A star HR 465 taken in late 2013 during program 13346. Each line connects measurements of the autocorrelation width for the same spectral order as measured in a few separate observations. The 31 longest wavelength calibrated orders for each grating are shown. As the autocorrelation width also depends on the sharpness of the underlying stellar spectrum this width will vary from order to order even at fixed spectral resolution. The E140M observations show little evidence for a change in resolution with model focus except that the resolution appears a bit lower at the most negative focus value. The E230M results suggest slightly higher resolution towards negative focus, consistent with the offset seen for the E230M observations seen in Fig. 20

5 Impact of Focus Offset on STIS Science

The most noticable impact of the apparent focus offset is the loss of throughput and signal-to-noise for observers using small apertures. For the commonly used 0.2X0.06 and 0.2X0.09 apertures, throughputs 25% below expectations are not uncommon, with occasional losses of as much as 40% (Fig. 2). Most severely affected is the very small 0.1X0.03 aperture, where recent typical throughputs have below expectations by as much as 60%. There is, however, some suggestion that comparable losses in small apertures may also have been common prior to SM4 as well (e.g., see Fig. 8).

It is not possible to simply lower the small aperture throughputs adopted in the Exposure Time Calculator to compensate for the average focus, as a particularly well focused observation might then lead to a bright object violation or a saturated image. Jenkins & Tripp (2001) demonstrated that the STIS E140H echelle is capbable of resolving powers as high as 200,000 when used with the 0.1X0.03 aperture, but at the current time the difficulties in reliably predicting the throughput for this aperture make it very problematic to exploit this capability in practice.

In Cycle 24 about 24% of STIS exposure time requested use of apertures 0.1” or smaller in the dispersion direction. This amounts to about 339 orbits of HST time. Examination of the individual proposals suggests about ½ of these exposures are sufficienctly sensitive to throughput to have their science goals at least modestly affected by the focus offset. If the typical throughput loss is 20% below that estimated by the ETC, then the equivalent of about 34 orbits of additional time would be needed to compensate. A similar analysis of the Cycle 23 program gives an estimate of 15

orbits. This conservative analysis suggests that the mis-focus results in an average loss equivalent to an average of 25 orbits per cycle.

Observations that require very high levels of repeatability may also be adversely affected by out-of-focus data. This is especially true for transiting planet observations which often aim for accuracies of 1 part in 10^4. In addition to small effects on even the large aperture throughputs, subtle changes in the line-spread function correlated with orbital breathing could impact the subtraction of measurements made in and out of transit.

6 Conclusions and Recommendations

6.1 Summary of Measurements

- Clear aperture throughputs suggest the best focus at the aperture plane has been offset significantly towards negative focus values with the maximum throughput occurring at focus values as low as –6 microns of equivalent secondary motion, since at least 2014. Insufficient suitable data exist to make definitive statements regarding the small aperture throughput as a function of focus at earlier times; however, there may already have been an offset of about –4 microns as early as 2001.
- Phase retrieval of STIS narrow-band OII images suggest that the focus has been drifting with respect to the standard HST focus model by about +1.25+\-0.15 microns per year since 2011. This is about the time after which the HST focus model added an extra secular shrinkage term of -1.55 microns/year. That is, STIS seems to be seeing a significantly smaller OTA shrinkage than is suggested by the standard observatory monitoring using ACS and WFC3.
- The baseline focus value from older OII ACCUM observations suggests a mean offset from best HST focus equivalent to –6.5 microns for this mode, while ACQ observations with the same filter suggest a baseline closer to -5 microns. It is likely that the ACCUM images produce more reliable results, and this is confirmed by the analysis of Lallo (private communication), which estimated from comparison of STIS and WFPC2 images that the offset in 2000 was –7.2±0.44 microns.
- Comparison of phase retrievals done for parallel STIS, ACS, and WFC3 observations suggests that the current offset between the STIS OII filter and the best observatory focus has changed from the historical values near –7.2 to –6.5 microns and is now close to –3.5 microns. While significant, this change is much less than that suggested by direct comparison with the observatory focus model.
- Autocorrelation of internal lamp exposures shows no evidence for internal STIS alignment changes over time.
- Measurements of the spectroscopic focus at the detector using autocorrelation comparisons for external targets show mixed results:
    - CCD 1st order modes show best focus close to zero for pre-SM4 and early post-SM4 data. Later data suggest that the best focus is moving towards more negative focus values, although with large visit-to-visit scatter.

- A limited number of autocorrelation results for the E230M grating suggest that its best focus may be at more negative settings than that found for 1st order CCD modes at similar epochs.
- Other modes lack sufficient data to give clear autocorrelation results.

Most likely STIS was for the bulk of its on-orbit lifetime not actually centered at the best aperture plane focus for unfiltered slits, but was offset by the equivalent of about –3 microns of secondary mirror motion. When the observatory monitoring indicated an increased OTA shrinkage rate starting in 2011, STIS appears to have followed a different trend, seeing a shrinkage rate much closer to the older behavior. As the observatory focus was adjusted to track the WFC3/ACS measurements STIS was left behind and is now shifted an additional ~ –3 microns from the best aperture plane focus, resulting in noticeably decreased small aperture throughputs.

As the internal alignment of STIS appears unchanged, any physical change in the STIS focus with respect to other instruments would appear to be due to a movement of either the STIS corrector or of the entire instrument. While it is difficult to rule out such alignment changes, there is also not an obvious explanation for the coincident timing of the alignment changes and the increased OTA shrinkage rate, suggested by the observatory monitoring. It may be worthwhile to also reconsider the observatory focus monitoring itself. For example, if those measurements switched from systematically overestimating the focus by about +1.5 microns to underestimating it by about the same amount, this could explain the STIS results without having to invoke any physical shift of the instrument or its corrector. We plan to repeat the parallel STIS/WFC3/ACS observations of 47 Tuc, (visit P2 of 14063 and 14425), in Cycle 24 and this should give additional information on the stability of the STIS focus relative to that of the other imaging instruments.

6.2 Recommendations

In principle, the STIS corrector mechanism could be moved to change the focus of STIS relative to the other instruments. While the mechanism has not been activated since the original SMOV period in 1997, re-powering the mechanism now should be relatively low risk. However, the same power supplies used for the corrector mechanism are needed for movement of most other STIS mechanisms, and a failure in these power supplies would render STIS completely incapable of taking science observations.

If the corrector were to be adjusted, a decision would also need to be made whether to simply remove the approximately 3 microns of additional offset that apparently has accumulated in recent years, or whether to make a larger offset to optimize throughput at the STIS aperture plane. This is complicated by the limited data available on the relative focus offsets between the various STIS modes.

If it were decided to go ahead with a focus adjustment, we would recommend beginning with a relatively conservative approach, with an emphasis on understanding the effects of any focus change on the resolution of the STIS first-order CCD spectra, which are heavily used for transiting planet observations where a high level of repeatability is required. We also recommend against over-reliance on the focus breathing model, as we have seen that individual visits may deviate

significantly from this model and this could lead to misleading conclusions from a focus sweep that depended on a small number of visits executed over a short period of time.

First the focus mechanism telemetry sensors should be activated to allow the current corrector focus and tip-tilt positions to be measured and compared with the expected values. Initially this should be done without any attempt to actually move the mechanisms. This will verify that the mechanisms are still where they were left in 1997, and allow any necessary updates of the flight software parameters to reflect the change from the STIS side-1 to side-2 electronics that occurred in 2001. Any move of the focus mechanism itself would be deferred until these results are understood.

We then suggest that an initial focus sweep be done using interleaved G430L and F28X50OII observations of a target that has been demonstrated to give clean auto-correlation results that can show resolution changes as a function of typical orbital breathing (e.g., HD 189733, as shown in Fig. 16). Interleaving the imaging and spectral observations will allow the resolution results to be cleanly tied to the phase retrieval focus measurements without having to depend on the reliability of the observatory focus model for a particular set of observations. Typical orbital breathing can lead to peak-to-peak focus variations of about 5 microns of secondary motion over the course of the orbital visibility (e.g., Figs. 11-13). A sequence of three orbits with the focus position first at the current position, and then with the focus mechanism offset by +302 motor steps (-3 microns), and then by +603 motor steps (-6 microns), should allow the full needed range to be mapped out, especially if the observations are scheduled with the target at an attitude and time expected to give typical breathing behavior as described by Hershey et al. (1998).

The results discussed above suggest that the best focus in the aperture plane is offset significantly towards a more negative focus value than the best focus for first order CCD modes. The results of the initial G430L + OII sweep would be used to select the most negative focus position consistent with acceptable G430L focus performance, and then a pair of confirmation visits would be done at the current and the proposed new focus values to verify that the small aperture throughput is improved at the new focus value. These observations would consist of peakups and ACCUM images using the 0.1X0.09 aperture. These observations should also be interleaved with OII images to ensure that the G430L autocorrelation results and the small aperture throughput measurements are tied to a common scale.

The timing of any change in the STIS focus position used for GO observations should take into account those observations which may depend sensitively on focus values. In particular, paired visits of transiting planet observations using the same target and CENWAVE setting that are intended to be directly compared with each other should if possible be executed using the same focus setting.

Additional autocorrelation sweeps with other STIS gratings might also be considered, but the large number of modes and the challenge of finding targets that can be verified to give good autocorrelation results at very high spectral resolution, with sufficiently short exposure times, might require a very substantial number of orbits and more analysis effort than is practical. As an example, for the E140H 1416 setting

the target HD 24534 might be a good choice as there are extensive observations using the 0.1X0.03 aperture that show a number of strong narrow molecular CO lines in this star's spectrum. An autocorrelation of these spectral regions as observed through the 0.2X0.2 aperture during a focus sweep might be used to determine the focus of the best E140H spectral resolution. The ETC predicts that this star is close to or perhaps a few percent above the normal 200,000 c/s bright object screening limit usually applied to STIS MAMA observations and so may provide a "best case" for further evalulation of the feasiblity of such a study.

In the absence of a focus move, we suggest continued monitoring of small aperture throughputs and autocorrelation results of suitable GO observations to identify any new trends that might indicate any further degradation of performance.

Uncertainties in the HST Observatory focus model also affect the ability to rely on OII phase retrieval to detect the presence of new trends. Any improvements in the understanding of the behavior and reliability of the secular and breathing corrections supplied in such models would be very valuable for this work as well.

Acknowledgements

Change History for STIS ISR 2017-01

Version 1: 12 January 2017 – Original Document

References

Bohlin, R. C., Gordon, K. D., & Tremblay, P.-E. 2014, PASP 126, 711

Bowers, C.W., Woodgate, B.E., Kimble, R.A. et al. 1998, SPIE Vol. 3356, 401

Di Nino, D., Makidon, R. B., Lallo, M. et al. 2008, Instrument Science Report, ACS 2008-03, "HST Focus Variations with Temperature"

Ebbets, D. 1995, Ball Systems Engineering report SER STIS CAL-018, "Filtered Aperture Image Displacements"

Hershey et al. 1998 STScI SESD-97-01, "Modeling HST Focal-Length Variations"

Jenkins, E. B., & Tripp, T. M. 2001, ApJS, 137, 297

Kimble, R. A. et al. 1998, ApJ 492, 492L

Krist, J. E. and Burrows, C. J.: 1997, STScI Phase Retrieval Software (FITPSF) User's Guide

Krist, J. E. and Burrows, C. J.: 1995, Applied Optics, 34, 4951, http://www.stsci.edu/institute/org/telescopes/Reports/AppliedOpticsHSTPhaseRetrieval.pdf

Lallo, M, Gilliland, R., & Hershey, J., Memorandum on OTA Focus Review & Status Entering SMOV3A, version 3 (http://www.stsci.edu/hst/observatory/documents/performsum/SMOV3Afocus2.memo.pdf)

Lallo, M., Makidon, R.B., Casertano, S., Gilliland, R., & Stys, J. Instrument Science Report TEL 2005-003

Lennon, D., Oliveria, C, Hartig, G. et al. 2010, Instrument Science Report COS 2010-07

Nichols, J. S., & Linsky, J. L. 1996, AJ, 111, 517

Niemi, S.-M., & Lallo, M. 2010 Instrument Science Report TEL 2010-01, "Phase Retrieval to Monitor HST Focus: II. Results Post-Servicing Mission 4"
Woodgate, B. E., et al. 1998, PASP, 110, 1183

Appendix: Samples of Phase Retrieval Input Parameter Files

Examples of input parameter files used with the Krist and Burrows (1995) procedure are shown below. Note that quantities labeled with a "Y" in the first column are those parameters that the fitting procedures allows to vary freely to find the best fit. Values labeled with "N" are held fixed, while values labeled with "I" are not used.

STIS OII Input File

```
      Array dimensions      512
            Wavelength   0.3740
        Fitting method        1
  Merit function power  2.00000
    Merit wing damping  0.00500
           Camera mode    STISCCD
          Zernike type OBSCURED
Y                   Focus (microns)       0.0000
Y                  X-coma (microns)       0.0000
Y                  Y-coma (microns)       0.0000
Y           X-astigmatism (microns)    0.0035831
Y           Y-astigmatism (microns)     0.015453
N               Spherical (microns)    -0.021103
N                X-clover (microns)   -0.0036286
N                Y-clover (microns)    -0.017079
I X-spherical astigmatism (microns)       0.0000
I Y-spherical astigmatism (microns)       0.0000
I               X-ashtray (microns)       0.0000
I               Y-Ashtray (microns)       0.0000
I   Fifth order spherical (microns)       0.0000
I              Pixel size (microns)       21.000
I                X-jitter (microns)       0.0000
I                Y-jitter (microns)       0.0000
I            Jitter angle (degrees)       0.0000
Y            Star  1 Background*1e4       0.0000
Y          Star  1 X-tilt (microns)       0.0000
Y          Star  1 Y-tilt (microns)       0.0000
N               Lyot stop X radius      0.82204
N               Lyot stop Y radius      0.86029
N               Lyot stop X offset     0.041447
N               Lyot stop Y offset     0.032098
```

WFC3 UVIS1 F410M Input File

```
      Array dimensions      512
            Wavelength   0.4107
        Fitting method        1
  Merit function power  2.00000
    Merit wing damping  0.00500
           Camera mode    WFC3UVIS1
          Zernike type OBSCURED
Y                   Focus (microns)       0.0000
Y                  X-coma (microns)       0.0000
Y                  Y-coma (microns)       0.0000
Y           X-astigmatism (microns)       0.0000
Y           Y-astigmatism (microns)       0.0000
Y               Spherical (microns)      -0.0110
N                X-clover (microns)       0.0035
N                Y-clover (microns)      -0.0065
```

```
I X-spherical astigmatism (microns)       0.0000
I Y-spherical astigmatism (microns)       0.0000
N               X-ashtray (microns)       0.0045
N               Y-Ashtray (microns)      -0.0065
I   Fifth order spherical (microns)       0.0000
Y            Star  1 Background*1e4       0.0000
Y          Star  1 X-tilt (microns)       0.0000
Y          Star  1 Y-tilt (microns)       0.0000
Y                             Blur       0.4500
```

ACS WFC2 F502N Input File

```
      Array dimensions      512
            Wavelength   0.5020
        Fitting method        1
  Merit function power  2.00000
    Merit wing damping  0.00500
           Camera mode    ACSWFC2
         Zernike type OBSCURED
Y                    Focus (microns)       0.0010
Y                  X-coma (microns)       0.0000
Y                  Y-coma (microns)       0.0000
Y           X-astigmatism (microns)       0.0000
Y           Y-astigmatism (microns)       0.0000
N               Spherical (microns)      -0.0139
N                X-clover (microns)      -0.0040
N                Y-clover (microns)       0.0100
I X-spherical astigmatism (microns)       0.0000
I Y-spherical astigmatism (microns)       0.0000
N               X-ashtray (microns)      -0.0050
N               Y-Ashtray (microns)       0.0030
N   Fifth order spherical (microns)       0.0050
Y            Star  1 Background*1e4       0.0000
Y          Star  1 X-tilt (microns)       0.0000
Y          Star  1 Y-tilt (microns)       0.0000
N             Spider rotation (deg)       0.0000
Y                             Blur       0.3275
```

ACS WFC1 F502N Input File

```
      Array dimensions      512
            Wavelength   0.5020
        Fitting method        1
  Merit function power  2.00000
    Merit wing damping  0.00500
           Camera mode    ACSWFC1
         Zernike type OBSCURED
Y                    Focus (microns)       0.0000
Y                  X-coma (microns)       0.0000
Y                  Y-coma (microns)       0.0000
Y           X-astigmatism (microns)       0.0000
Y           Y-astigmatism (microns)       0.0000
N               Spherical (microns)      -0.0139
N                X-clover (microns)      -0.0040
N                Y-clover (microns)       0.0100
I X-spherical astigmatism (microns)       0.0000
I Y-spherical astigmatism (microns)       0.0000
N               X-ashtray (microns)      -0.0050
N               Y-Ashtray (microns)       0.0030
N   Fifth order spherical (microns)       0.0050
Y            Star  1 Background*1e4       0.0000
Y          Star  1 X-tilt (microns)       0.0000
Y          Star  1 Y-tilt (microns)       0.0000
N             Spider rotation (deg)       0.0000
Y                             Blur       0.3710
```